Available online at www.sciencedirect.com
SCIENCE DIRECT®
International Journal of Thermal Sciences 42 (2003) 703–711
International Journal of Thermal Sciences
www.elsevier.com/locate/ijts

Wall air–jet characteristics and airflow patterns within a slot ventilated enclosure

Jean Moureh [a,*], Denis Flick [b]

[a] *Refrigerating Process Engineering Unit, Cemagref-BP 44, 92163 Antony cedex, France*
[b] *INA-PG, 16, rue Claude Bernard, 75005 Paris, France*

Received 26 November 2001; accepted 31 August 2002

Abstract

The present study reports on the numerical and experimental characterisation of airflow generated by a wall jet within a long and empty slot-ventilated enclosure. In the configuration investigated, blowing and outlet sections are placed in the front of the box. This design is extensively used in refrigerated transport. Experiments were carried out on a scale model (1 : 3.3) of a trailer. Numerical modelling of airflow was performed using the computational fluid dynamics Fluent code. In this study, a second-moment closure, the Reynolds stress model (RSM) and two-equation turbulence models: the standard k–ε and a renormalization group (RNG), were tested, contrasted and compared with experimental data. It was demonstrated that only the RSM model enabled detection of the presence and the localisation of separated flow and correctly predicts airflow patterns related to primary and secondary recirculation.

Keywords: Slot-ventilated; Airflow; Laser; Ventilation; CFD; Modelling

1. Introduction

Slot-ventilated enclosures are extensively used in many engineering applications in order to control the level and the homogeneity of temperature, concentrations and contaminants in the confined space. All these parameters are strongly governed by the airflow patterns and their distribution into the room.

Many investigations are carried out to characterize the behaviour of airflow in the ventilated room as a function of slot and room dimensions and the positions of inlet and outlet sections [1–4].

Although the positioning of blowing and outlet sections varies generally, these are located face to face within the ventilated space [3–7]. This design, when it can be achieved, ensures better domain occupancy considered by the main flow and thus reduces the importance of the secondary recirculating zones, in which the low rate of air renewal increases the temperature difference.

This paper considers the particular case of an empty slot-ventilated room, for which inlet and outlet sections of airflow are located on the same side. From an aerodynamic standpoint, the drawback of this asymmetrical design is the presence of a strong pathway between the two sections, implying high velocities at the front section and low velocities at the rear part of the enclosure. The major configurations investigated [1,2] are short to moderate length ($L/H \leqslant 2$, where L is the room length, and H is the room height). In addition, these configurations consider only the case of ceiling air–jet for which the slot inlet width is equal to the width of the room.

The results given by Yu and Hoff [2] reveals the presence of a reverse flow in the rear opposite face. The author explains the presence of this secondary flow by the detachment of the wall jet from the ceiling. The airflow field and the location of the detachment point of the ceiling air jet were shown to be independent of airflow rate beyond a threshold value. The pressure data obtained by Karimipanah [1] along the ceiling reveals the presence of an adverse pressure near the opposite wall. However, the influence of this adverse pressure on the airflow patterns was not investigated.

The case of a long enclosure is generally encountered in refrigerated transport where blowing and exit sections

* Corresponding author.
E-mail addresses: jean.moureh@cemagref.fr (J. Moureh), flick@inapg.inra.fr (D. Flick).

1290-0729/03/$ – see front matter
doi:10.1016/S1290-0729(03)00037-1

Nomenclature

p	static pressure	Pa
U_i, u_i	mean, fluctuating velocity component in x_i direction	$m{\cdot}s^{-1}$
Q	flow rate	$m^3{\cdot}s^{-1}$
L	length of the enclosure	m
H	height of the enclosure	m
I	turbulence intensity	%
P	production term	$m^2{\cdot}s^{-3}$
x, y, z	lateral, vertical and longitudinal coordinates	m
C_μ, C_1, C_2	turbulence model coefficients	
D_H	Hydraulic diameter of the inlet section	m
Re	Reynolds number, $= \rho U_0 D_H/\mu$	
y^+	dimensionless wall unit, $= (\tau_w/\rho)^{0.5} y/\nu$	
T, t	mean, fluctuating temperature	K
τ_w	wall shear stress	Pa

Greek symbols

ρ	density	$kg{\cdot}m^{-3}$
σ_k, σ_ε	turbulent diffusion coefficients for k and ε, respectively	
ν	kinematic viscosity	$m^2{\cdot}s^{-1}$
μ	dynamic viscosity	$kg{\cdot}m{\cdot}s^{-1}$
k	kinetic energy of turbulence	$m^2{\cdot}s^{-2}$
ε	turbulence energy dissipation rate	$m^2{\cdot}s^{-3}$

Subscripts

0	inlet
m	maximum
t	turbulent
i, j, k	vector directions

of airflow are located on the anterior face since it is very practical to place all the refrigerated equipment together near the refrigerating unit. However, the temperature differences observed by many authors [8,9] in the case of a loaded configuration cannot be directly exploited in this study because of the combined effect of the compactness of the load and to the asymmetrical design of the airflow system. Consequently, the case of an empty enclosure without the influence of the load needs to be investigated first.

The objective of the present study is to investigate experimentally and numerically the behaviour of airflow patterns, velocity characteristics and temperature distribution within a long and empty slot-ventilated enclosure for which inlet and outlet sections are placed on the same side. Analysis of experimental and numerical data should identify the mechanisms governing the maintaining on the ceiling of the confined jet or its separation, its reach, the importance of the primary jet zone and any secondary flows.

Concerning the use of a turbulence model, many studies use the standard k–ε model [10] since it is easy to programme and can be broadly applied. However, predictions given by this model are not often accurate and ad-hoc modifications are performed in order to improve the computed results.

In order to better predict the airflow pattern in a ventilated enclosure with a strong Coanda-effect influence, Choi [7] suggests modifying the multiplicator coefficient $C_\mu = 0.09$ of the turbulent viscosity given by the standard k–ε model. The author recommends, respectively, $C_\mu = 0.12$ and 0.15 if the blowing is near or far from the ceiling. However, the fact that this model thus modified cannot be universally applied will discourage further use without comparative experimental data.

Even though the use of low Reynolds numbers (LRN) models is recommended by many authors [11,12], Hoff [6] shows that use of the Lam et Bremhost [13] model overpredicts the Coanda effect. This can lead to poor prediction concerning the maintaining of the jet on the ceiling, its reach and to the occurrence of secondary flow. In addition, for certain low-velocity recirculating zones, where laminar and turbulent phenomena exist locally, not only in the near wall region, but also remote from walls, using the LRN k–ε model often indicates unrealistic laminar solutions [5]. Moreover, as very fine grid distribution is needed in the near-wall region, the computing time and memory storage cost are significantly higher when using high-Reynolds-number models. These aspects constitute the principal limitation for LRN models.

In a comparison concerning different k–ε models for indoor airflow, Chen [14] shows that either of these two equation models is able to predict the presence of secondary recirculating flow. The fact that the turbulence model cannot be universally applied has been a frequent criticism. Discrepancies between predicted results and measured data are difficult to identify. Airflow in a room is complicated: it is often the combination of free turbulent shear flows, near wall effect, pressure gradient implying the presence of separating and reattaching jet, primary and secondary recirculating including high streamline curvature effect [3–7,14]. For these complex flows, various authors [1,15–17] agree on the inadequacy of the k–ε model to predict airflow patterns and underline its limitation by comparison with experimental data. In this case, improving predictions can be achieved by taking into account the effect of the turbulence anisotropy by using second-moment closure [1,3].

According to the complexity of the airflow in a room, rigorous validation for numerical models is needed before they can be applied to wide ranging air distribution problems. This validation concerns primarily the choice of a turbulence model for which it is necessary to investigate its performance by comparing numerical predictions with experimental data. For the case studied, two levels of turbulence modelling are

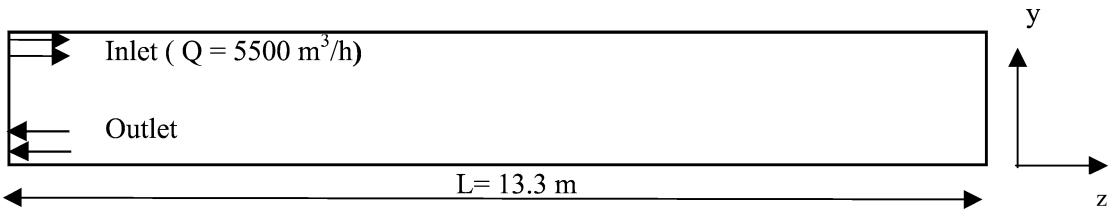

Fig. 1. Longitudinal view of the slot-ventilated enclosure.

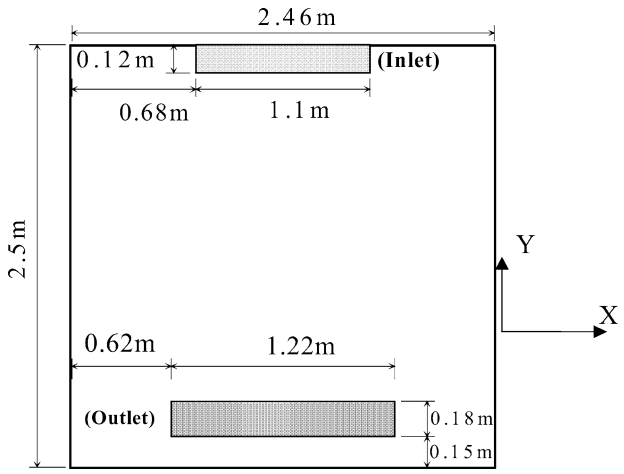

Fig. 2. Cross-section showing inlet and outlet positions and dimensions.

performed. The second-moment closure with the Reynolds stress model as described by Launder et al. [18] and two basic two-equation models: the standard k–ε and a renormalization group (RNG) [19].

2. Experimental device

The experiments were carried out using a reduced-scale (1:3.3) model of a truck enclosure with respect to the adimensional Reynolds number ($Re = \rho U_0 D_H/\mu$). Afterwards, all the data: dimensions, flow rate and results, are expressed for the actual scale (Figs. 1 and 2). The air is supplied through a small inlet section located adjacent to or near the ceiling, at a relatively high velocity. Due to the Coanda effect, this design should allow to the issuing confined wall jet to adhere, as far as possible, to the ceiling and to improve the ventilation efficiency on the whole enclosure.

The walls of the scale model are made of wood. Only one lateral wall is made of glass to allow internal air velocity measurement using laser Doppler velocimetry. The blowing and outlet sections are located on the same side at the front of the trailer.

The determination of mean velocity and its fluctuation was performed using a laser-Doppler anemometer. It comprised a 50 mW laser diode emitting a visible red beam at 690 nm wavelength, a Beamsplitter, a Brag cell, a focussing and receiving lens and a pinhole arrangement to collect scattered light from within the measurement value and a photomuliplier. Light scattered from particles is captured through the same front lens that the two beams exit from. The air supplied to the model trailer was passed through atomizers and allowed near continuous Doppler signals which were converted into velocity and time. In these experiments, the decay of the velocity along the enclosure and vertical profiles at 1, 2 and 4 m are obtained. In addition to these profiles, 1080 measurements for horizontal and vertical velocities are performed in the whole medium/symmetry plane in order to represent the streamlines and airflow pattern.

3. Numerical modelling

3.1. Governing equations and hypothesis

The description of temperature and air flow development are based on the conservative law of mass, motion and energy. Natural convection is considered by using the Boussinesq approximation in which density was treated as a constant value in all solved equations except for the buoyancy term in the momentum equations which was treated as: $(\rho_0 - \rho)g = \rho_0\beta(T - T_0)g$, where ρ_0 and T_a are the reference density and temperature, respectively, and β is the thermal expansion coefficient. The solved equations can be written as follows:

Mass conservation:

$$\frac{\partial U_j}{\partial x_j} = 0 \tag{1}$$

Momentum conservation:

$$\frac{\partial U_j U_i}{\partial xj} = -\frac{1}{\rho}\frac{\partial P}{\partial x_i} + \frac{(\rho_0 - \rho)}{\rho_0} g\delta_{i3} + \frac{\partial}{\partial x_j}\left(\nu\frac{\partial U_i}{\partial x_j} - \overline{u_i u_j}\right) \tag{2}$$

Energy conservation:

$$\frac{\partial U_j T}{\partial x_j} = \frac{\partial}{\partial x_j}\left(\overline{u_j t}\right) \tag{3}$$

where $\overline{u_i u_j}$ and $\overline{u_j t}$ are, respectively, the unknown Reynolds stresses and heat fluxes. The obtaining of these quantities depends on the turbulence closure. For the case investigated, two levels of turbulence modelling closure have been employed:

– on one hand with two-equation models: the standard k–ε and the renormalization group (RNG), based on the Boussinesq hypothesis;
– on the other hand with a second-moment closure with the Reynolds stress model (RSM).

3.1.1. The standard k–ε model

Using the Boussinesq hypothesis, the Reynolds stresses can be described as follows:

$$-\overline{u_i u_j} = \nu_t\left(\frac{\partial U_i}{\partial x_j} + \frac{\partial U_j}{\partial x_i}\right) - \frac{2}{3}k\delta_{ij} \tag{4}$$

the eddy (turbulent) viscosity ν_τ is obtained from:

$$\nu_t = C_\mu \frac{k^2}{\varepsilon}$$

The turbulence kinetic energy k and the dissipation rate ε are determined using the following transport equations, respectively:

$$U_i\frac{\partial k}{\partial x_i} = \frac{\partial}{\partial x_i}\left[\left(\nu + \frac{\nu_t}{\sigma_k}\right)\frac{\partial k}{\partial x_i}\right] + P_k - \varepsilon \tag{5}$$

$$U_i\frac{\partial \varepsilon}{\partial x_i} = \frac{\partial}{\partial x_i}\left[\left(\nu + \frac{\nu_t}{\sigma_\varepsilon}\right)\frac{\partial \varepsilon}{\partial x_i}\right] + \frac{\varepsilon}{k}(C_1 P_k - C_2\varepsilon) \tag{6}$$

P_k represents the shear production term:

$$P_k = \nu_t\left[\frac{\partial U_i}{\partial x_j} + \frac{\partial U_j}{\partial x_i}\right]\frac{\partial U_i}{\partial x_j} = \nu_t S^2 \tag{7}$$

where S represents the modulus of the mean rate-of-strain tensor, defined as:

$$S \equiv \sqrt{2S_{ij}S_{ij}}, \qquad S_{ij} = \frac{1}{2}\left(\frac{\partial U_i}{\partial x_j} + \frac{\partial U_j}{\partial x_i}\right) \tag{8}$$

The model coefficients in the standard k–ε model are:

$$(C_\mu, C_1, C_2, \sigma_k, \sigma_\varepsilon) = (0.09, 1.44, 1.92, 1.0, 1.3)$$

3.1.2. The renormalization group k–ε model

The RNG-based k–ε turbulence model is derived from the instantaneous Navier–Stokes equations, using a mathematical technique called "renormalization group" (RNG) methods. The analytical derivation results in a model with constants different from those in the standard k–ε model, and includes an additional source term R in the transport equation of the dissipation-rate defined as:

$$R = C_\mu \frac{\eta^3(1-\eta/\eta_0)}{1+\beta\eta^3}\frac{\varepsilon^2}{k}$$

$$\eta = S\frac{k}{\varepsilon}$$

The version used is that of Yakhot and Orszag [19] (hereafter denoted RNG k–ε is used). The model coefficients in the RNG k–ε model are:

$$(C_\mu, C_1, C_2, \sigma_k, \sigma_\varepsilon, \eta_0, \beta) = (0.0845, 1.42, 1.68, 0.7194, 0.7194, 4.38, 0.012)$$

3.1.3. RSM model

The obtaining of the transport equations for Reynolds turbulent stress is performed by subtracting the product of the mean velocities by the time-averaged Navier–Stokes equations from the product of instantaneous velocities by instantaneous Navier–Stokes equations. This gives rise to:

$$U_k\frac{\partial \overline{u_i u_j}}{\partial x_k} = -\frac{\partial}{\partial x_k}\left[\overline{u_i u_j u_k} + \frac{p}{\rho}(\delta_{kj}u_i + \delta_{ik}u_j) - \nu\frac{\partial(\overline{u_i u_j})}{\partial x_k}\right] + P_{ij} - \overline{\frac{p}{\rho}\left[\frac{\partial u_i}{\partial xj} + \frac{\partial u_j}{\partial xi}\right]} - 2\nu\overline{\frac{\partial u_i}{\partial x_k}\frac{\partial u_j}{\partial x_k}} \tag{9}$$

where

$$P_{ij} = -\overline{u_i u_k}\frac{\partial U_j}{\partial x_k} - \overline{u_j u_k}\frac{\partial U_i}{\partial x_k}$$

represents the production term.

The diffusive transport term was represented by a simplified form of the generalized gradient diffusion hypothesis as:

$$-\frac{\partial}{\partial x_k}\left[\overline{u_i u_j u_k} + \frac{p}{\rho}(\delta_{kj}u_i + \delta_{ik}u_j) - \nu\frac{\partial(\overline{u_i u_j})}{\partial x_k}\right] = \frac{\partial}{\partial x_k}\left(\frac{\nu_t}{\sigma_k}\frac{\partial}{\partial x_k}(\overline{u_i u_j})\right) \tag{10}$$

The pressure-strain term consisted of the linear return-to-isotropy and is modelled by Launder et al. [20] as:

$$\overline{\frac{p}{\rho}\left[\frac{\partial u_i}{\partial xj} + \frac{\partial u_j}{\partial xi}\right]} = -C_1\frac{\varepsilon}{k}\left[\overline{u_i u_j} - \frac{2}{3}\delta_{ij}k\right] - C_2\left[P_{ij} - \frac{2}{3}\delta_{ij}P\right] \tag{11}$$

where the constants $C_1 = 1.8$ and $C_2 = 0.60$, and $P = 0.5P_{ii}$.

The dissipation term was assumed isotropic, and was approximated by:

$$2\nu\overline{\frac{\partial u_i}{\partial x_k}\frac{\partial u_j}{\partial x_k}} = \frac{2}{3}\delta_{ij}\varepsilon$$

where the dissipation rate was computed via the ε transport equation.

The turbulent heat fluxes was expressed as:

$$\overline{u_j t} = -\frac{\partial}{\partial x_j}\left(\frac{\nu_t}{Pr_t}T\right)$$

3.2. Boundary conditions

The computational domain may be surrounded by inflow and outflow boundaries in addition to symmetry and solid walls.

At the inlet, uniform distribution is assumed for velocity components, kinetic energy of turbulence k_0 and the energy dissipation rate, ε_0. The numerical values are specified as:

– ($U_{0x} = U_{0z} = 0$; $U_{0z} = U_0 = 11.5$ m·s^{-1} representing the mean streamwise longitudinal velocity, giving an inlet flow rate $Q_0 = 5500$ m^3·h^{-1};
– $T_0^* = 0$ and $T^*_{\text{external}} = 1$, the overall heat transfer coefficient through the enclosure's wall is considered as being equal to 0.3 W · m^{-2}·K^{-1};
– $k_0 = 3/2(U_0 I_{0z})^2$; where I_{0z} represents the turbulence intensity of the z-component of velocity at the inlet;
– $\varepsilon_0 = (C_\mu^{0.75} k_0^{1.5}/0.07 D_{\text{H}})$ where D_{H} represents the hydraulic diameter of the inlet section;
– for the RSM model, turbulence is assumed to be isotropic:

$$\overline{u_i u_j} = \frac{2}{3} k_0 \delta_{ij}$$

According to these conditions the Reynolds number is considered as being equal to 2×10^5 in experiments and numerical simulations.

At the outflow, pressure is supposed to be uniform and zero-gradient is applied for all transport variables.

The turbulence models are only valid in fully turbulent regions. Close to the wall, where viscous effects become dominant, the model is used in conjunction with wall functions. For this study, the conventional equilibrium logarithmic law governing the wall is used [12].

At the symmetry plane, zero normal velocity and zero normal gradients of all variables are assigned.

The computations were carried out using FLUENT, a commercial computational-fluid dynamics (CFD) code on a three-dimensional configuration. The governing equations are solved using the finite-volume method in a staggered grid system. Non-uniform grid distribution is used in this study, with finer grid in regions near the inlet, outlet and walls where high gradients are expected.

In these simulations, the quick scheme, based upon three-point upstream-weighted quadratic upstream interpolation rather than linear interpolation between consecutive grid points [20]. The principal objective in using the quick scheme is to reduce the grid size required to yield a grid-independent solution, in comparison to the low-order scheme.

In order to test the influence of the grid size on the solution, three types of the grid are tested:

– a relatively fine grid with $50 \times 52 \times 240$: depth (2.46 m) × height (2.5 m) × length (13.3 m) = 624 000 cells;
– a medium grid: $50 \times 52 \times 160$ (416 000);
– a coarse grid: $40 \times 42 \times 142$ (238 560 points).

In all figures presented below, the fine grid has been used unless otherwise stated.

4. Results and discussion

4.1. Airflow pattern analysis

In order to better understand the behaviour of the flow patterns within the enclosure, we represent in Fig. 3(a) the streamline related to the mean flow field in the symmetry plane. These streamlines are obtained from 1080 (24×45) measurements points made using the LDV system. On the same plane, Fig. 4 presents the decrease of the velocity from the middle of the blowing section. It can be seen that the wall

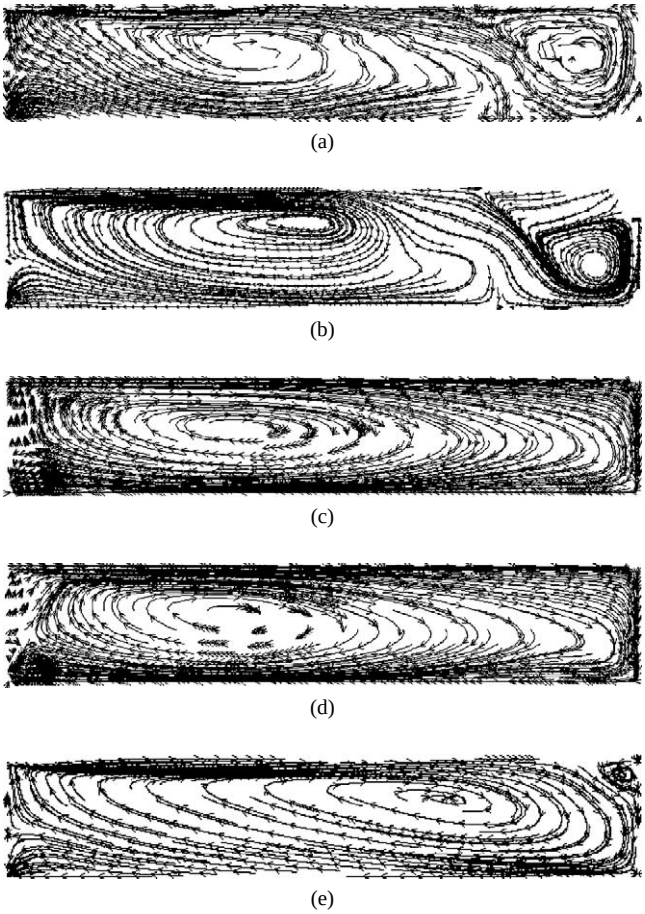

Fig. 3. Influence of the turbulence model and the grid size on the flow pattern at the medium plane: (a) Experiment; (b) RSM model; (c) k–ε; (d) RNG k–ε model; (e) RSM model with a coarse grid.

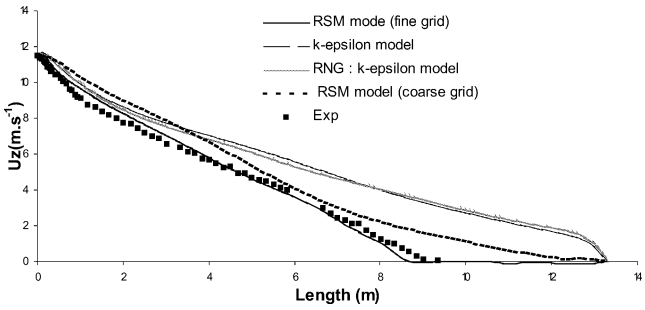

Fig. 4. Decay of the jet velocity along the enclosure.

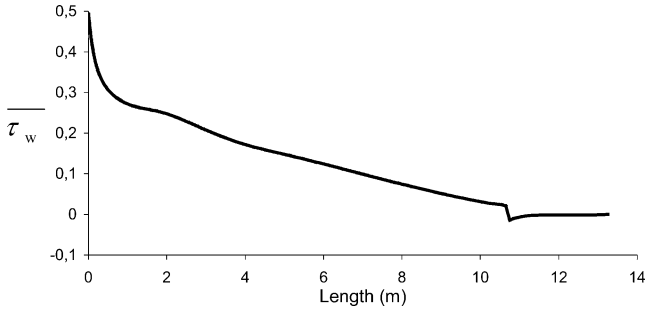

Fig. 5. Evolution of the wall shear stress on the ceiling along the enclosure.

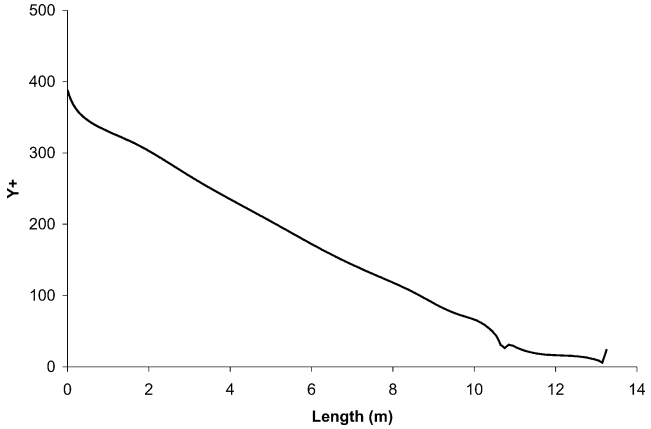

Fig. 6. Evolution of the wall y^+ on the ceiling along the enclosure.

jet separates from the ceiling at approximately 10 m from the inlet and reattaches at floor level.

This separation, whose mechanisms are discussed later, splits the jet into two regions dominated by two vortices of opposite circulation. The primary recirculation located on the front part of the enclosure delimits the reach and the action of the inlet jet. Conversely, the secondary flow located at the rear part is weakly supplied by the primary jet. In addition, the velocities are very low.

Figs. 5 and 6 show, respectively, the longitudinal evolution of the wall shear stress along the enclosure on the ceiling and the y^+ quantity related to the adjacent first cell. Due to marked variations in velocity along the enclosure, y^+ varies from 380 at the blowing to 10 on the rear of the vehicle. At the separation point, the wall shear stress vanishes and y^+ shows slight discontinuity. But we should note that at this point, the logarithmic law of the wall is not valid.

4.2. Thermal field

Fig. 7 represents a contour plot of adimensionnal temperature distribution (T^*, which is defined as: $T^* = (T - T_0)/(T_{\text{outlet}} - T_0)$). It can be seen that in the primary recirculating area T^* is below or equal to 1. This reflects high ventilation efficiency without stagnant zones as encountered in piston flow. Conversely, at the rear of the enclosure where secondary recirculation dominates, T^* reaches high values which indicates a low ventilation efficiency.

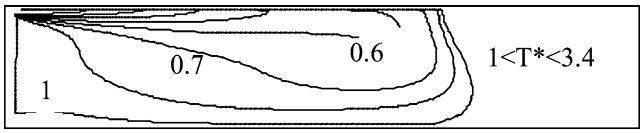

Fig. 7. Contour plot of adimensionnal temperature distribution ($T^* = (T - T_0)/(T_{\text{exit}} - T_0)$).

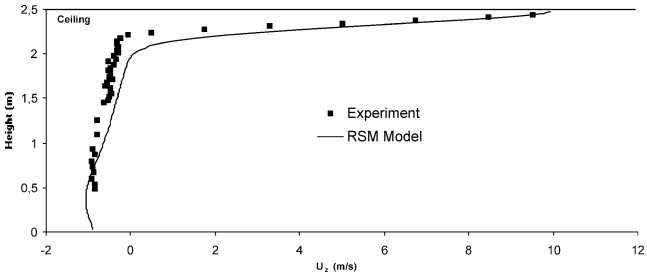

(a)

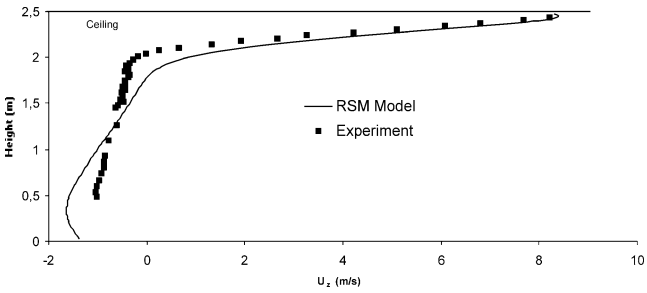

(b)

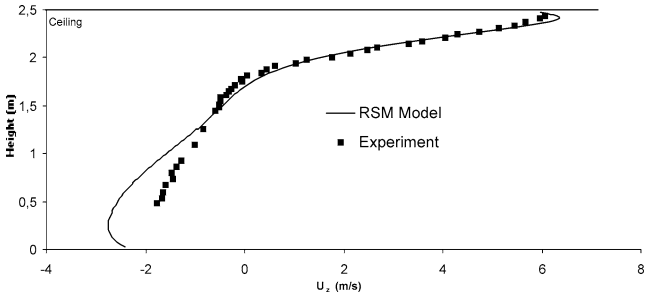

(c)

Fig. 8. Vertical profiles of horizontal velocities: (a) 1 m; (b) 2 m; (c) 4 m.

4.3. Turbulence modelling performance

In order to better understand the mechanisms governing the diffusion of the confined jet in the enclosed area, it is necessary to investigate, in addition to experimental data, numerical data since the latter are more complete. Before use, it is essential to validate the model by comparisons with experimental data. In order to perform this step correctly, we carried out comparisons on both local velocity measurements and the global behaviour of the airflow patterns.

Fig. 3(b), (c) and (d) show the streamline predictions obtained by k–ε, RNG and RSM for the fine grid. Only the RSM model shows the ability to catch the secondary recirculation and to predict correctly the general behaviour of air motion related to the primary and to the second recircula-

tions. In addition, the predicted positions of detachment and reattachment points are very close to experimental data (see Fig. 3(a)). However, according to comparisons concerning velocity profiles reported in Fig. 8, the RSM model seems to overpredict to some extent the diffusive character of the jet near the inlet sections at 1 and 2 m. This trend can be due to a surestimated value of turbulence intensity at the inlet.

Although the RNG was successfully used to predict flow separation in an axisymmetric 180° narrowing bend by Luo [21], its predictions for the present geometry are similar to those of the k–ε model. It can be seen that neither model is able to predict flow separation. The poor predictions given by two-equation turbulence models (k–ε and RNG) can be explained by the overly diffusive character of these models. In addition, according to Wilcox [15] and Menter [16], the k–ε model predicts significantly too high shear-stress levels and thereby delays or completely prevents separation. According to Launder [22], this trend can be more pronounced in the presence of adverse pressure gradient and leads to overprediction of the wall shear stress. This implies the non-separation of the jet from the ceiling and leads to increased domination of the primary recirculation in the whole enclosure. This failure of the k–ε based models in predicting complex flows, including secondary and/or separated flows caused by adverse pressure gradient, was observed by many authors [14–16,21]. However, we should mention the good ability of the k–ε model to predict the abscissa of the detachment point with an accuracy within 10% for a non-isothermal wall jet supplied in an unbounded ambience [23]. But in this case, the detachment of wall jet is driven only by buoyant forces and is of an unavoidable nature.

4.4. Sensitivity to the grid size

The good predictions given by the RSM model (Fig. 3(b)) seem to be altered by using a coarse grid defined above. In this case (Fig. 3(e)), the detachment point is located more downstream and in turn the second recirculation area is reduced on the advantage of the primary recirculation. The altered RSM predictions become closer to k–ε based models ones. This behaviour can be explained by the increased of numerical diffusion due to the discretisation of the coarser grid.

Other data concerning the medium grid, not presented here due to lack of space, show that the predicted solution given by the fine grid is grid-independent.

Hereafter, only numerical data, obtained using the RSM model and the fine grid, will be used.

4.5. Comparison with a two-dimensional wall jet

Fig. 9 presents a comparison concerning the longitudinal velocity decay between the present configuration and a two-dimensional wall jet introduced in a free ambience ($p =$ constant). This jet was approximated by measurements performed by Meyers et al. [24]: $U_m/U_0 = 3.5/(x/h)^{0.5}$.

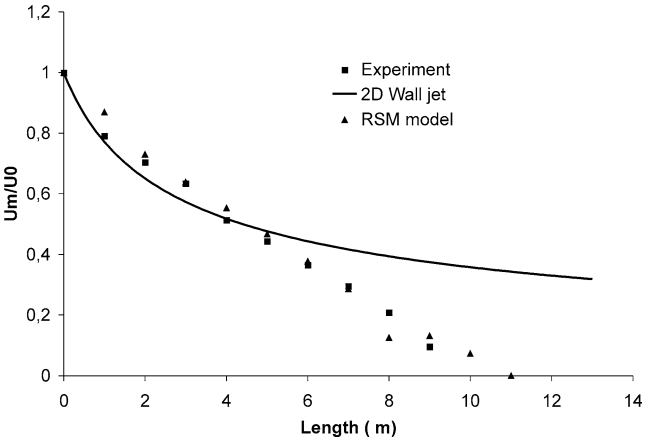

Fig. 9. Decay of the maximal velocity of the jet.

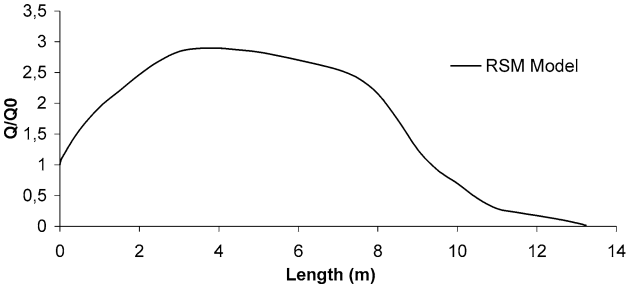

Fig. 10. Evolution of the flow circulation rate scaled by inlet flow rate through the enclosure.

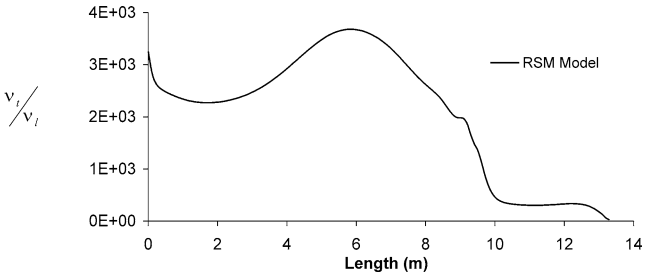

Fig. 11. Evolution of the turbulent viscosity ratio through the truck along the blowing medium line.

This comparison shows that the jet evolution in the confined enclosure is similar to a wall jet in a free ambience over $x/h = 50$, representing 5 m from the inlet section. This distance coincides with the centre of the primary flow recirculation which tends to reinforce the Coanda effect and the maintaining of the jet on the ceiling. This mechanism avoids the formation of a direct short-circuit between inlet and outlet sections. Beyond the centre of recirculation, the combined effect of this recirculation and the outlet tends to accelerate the decay of the wall jet and finally to separate it from the wall.

4.6. Aerodynamic behaviour of the two recirculating areas

To better illustrate the air flow characteristics of each recirculating area, Figs. 10 and 11 represent from numerical

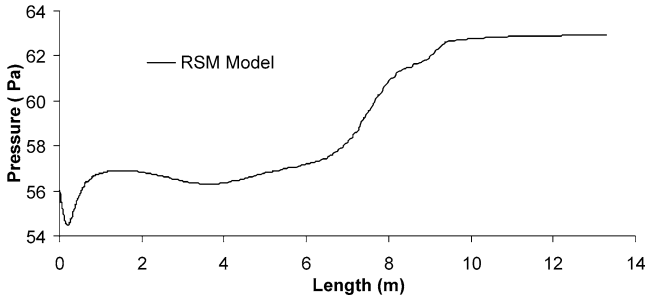

Fig. 12. Evolution of static pressure through the blowing medium line.

data given by the RSM model, the longitudinal evolution along the enclosure of the airflow rate scaled by the inlet flow rate ($Q(z)/Q_0$) and the turbulent viscosity tacked on middle of the blowing section. For a given cross-section along the enclosure, the circulating flow rate $Q(z)$ is calculated as:

$$Q(z) = 0.5 \int_{S_{(z)}} |U_z| \, \mathrm{d}s \tag{12}$$

- $S_{(z)}$: represents the considered cross-section at z coordinate;
- U_z: represents the local longitudinal velocity normal to $S_{(z)}$.

The results show a very net aerodynamic contrast between the two recirculating areas. The higher values of flow rate and turbulence viscosity related to the primary recirculating reflect respectively the importance of convective and diffusive mechanisms in this area compared with the secondary recirculating area. It can be seen that the flow rate of the primary recirculation is five times higher than the inlet flow rate and ten times higher than the second recirculating flow rate. Consequently the ventilation efficiency or the air changes per hour defined as the ratio between the inlet flow rate and the whole volume of the room, should be revised and adjusted locally as a function of the behaviour of airflow patterns and the evolution of the airflow circulation through the enclosure.

4.7. Flow separation analysis

If the maintaining of the blowing jet on the ceiling can be easily explained by the Coanda effect, its separation over a certain distance from the inlet necessitates analysing the external flow generated by the outlet and its impact on it. The reverse flow of the outlet implies generation of a positive pressure gradient ($\mathrm{d}p/\mathrm{d}z > 0$; z is oriented towards the rear). This gradient is favourable to the reverse flow and defavourable to blowing wall jet. Fig. 12 presents the evolution of the pressure along the enclosure. This evolution indicates the presence of a high positive (adverse) pressure gradient between 7 and 9 m that corresponds to the transition between the two recirculating areas.

Thus, the separating flow can be explained by the presence of an adverse pressure gradient. The separating area can be characterized by a certain balance in the horizontal direction among pressure gradient, inertia, viscous and turbulent stresses and in the vertical direction between Coanda effect and the normal pressure gradient caused by the outlet suction effect and the entrainment by recirculating flows. Therefore, the dynamic interaction between these different effects can probably explain the instability of the detachment point position since it oscillates around an average position. In this area, the velocity measurements are characterized by weak fluctuations in the order of 1 Hz consequently, the zones occupied by these recirculations expand and narrow at the rate of these fluctuations.

From a numerical standpoint, the use of averaged turbulence models does not allow prediction of the existence and the importance of these fluctuations. A better analysis taking into account the spatial-temporal character of these fluctuations necessitates the use of non-stationary turbulence models such as Large Eddy or Direct Numerical simulations. However, the drawbacks in terms of computing cost and memory storage could be too high, especially for the large space investigated.

5. Conclusion

In this study, experiments and numerical simulations were carried out in order to characterize velocities and airflow patterns inside within a long and empty slot-ventilated enclosure characterized by the presence of inlet and outlet sections on the same side at the front.

The experiments carried out on a reduced-scale model with a Laser Doppler velocimetry show a flow separation of the blowing wall jet along approximately two thirds of the total length of the enclosure. This separation splits the jet into two regions dominated by two vortices of opposite circulation. The RSM model readily predicts this flow separation. In addition, comparison with experimental data shows good overall agreement concerning positions of detachment and reattachment points, velocity curves and the global behaviour of airflow patterns. Conversely, the standard and the RNG k–ε based models fail to predict any flow separation.

The analysis of numerical results given by the RSM model shows that the convective, momentum diffusive and air-renewal mechanisms related to primary recirculation are significantly more important than concerning secondary flow recirculation. The flow rate of the primary recirculation is ten times higher than the second recirculating flow rate. This implies large temperature differences in the rear part of the enclosure. Consequently, air renewal requirements computed using actual averaged values of air changes per hour should be revised and adjusted according to the local values of airflow characteristics.

References

[1] M.T. Karimipanah, Deflection of wall–jets in ventilated enclosures described by pressure distribution, Building Environ. 34 (1999) 329–333.

[2] H. Yu, S.J. Hoff, Airflow pattern criteria for ceiling slot-ventilated agricultural enclosures under isothermal conditions, Amer. Soc. Agricultural Engrg. 42 (2) (1999) 459–469.

[3] H.B. Awbi, Application of computational fluid dynamics in room ventilation, Building Environ. 24 (1) (1989) 73–84.

[4] P.V. Nielsen, A. Restivo, J.H. Whitelaw, The velocity characteristics of ventilated rooms, J. Fluids Engrg. (1978) 291–298.

[5] L. Davidson, Ventilation by displacement in a three-dimensional room: A numerical study, Building Environ. 24 (1989) 263–272.

[6] S.J. Hoff, K.A. Janni, L.D. Jacobson, Three-dimensional buyant turbulent flows in a scaled model, slot-ventilated, livestock confinement facility, Amer. Soc. Agricultural Engrg. 35 (2) (1992) 671–686.

[7] H.L. Choi, L.D. Albright, M.B. Timmons, An application of the k–ε turbulence model to predict how a rectangular obstacle in a slot-ventilated enclosure affects air flow, Trans. Agriculture 33 (1) (1990) 274–281.

[8] R. Lindqvist, Reefer hold distribution, Preprint Conferences, IIF/IIR, Cambridge, UK, 1998.

[9] R. Lindqvist, Air distribution design for controlled atmosphere in reefer cargo holds, 20th International Congress of Refrigeration, IIR/IIF, Sydney, 1999.

[10] B.E. Launder, D.B. Spalding, The numerical computation of turbulent flows, Comput. Methods Appl. Mech. Energy 3 (1974) 269–289.

[11] H.C. Chen, V.C. Patel, Near wall-turbulence models for complex flows including separation, AIAA J. 26 (6) (1988) 641–648.

[12] V.C. Patel, W. Rodi, G. Scheuerer, Turbulence model for near-wall and low Reynolds number flows: A review, AIAA J. 23 (9) (1985) 1308–1319.

[13] C.K.G. Lam, K. Bremhorst, A modified form of the k–ε model for predicting wall turbulence, ASME J. Fluids Engrg. 103 (1981) 456–460.

[14] Q. Chen, Comparison of different k–ε models for indoor air flow computations, Numer. Heat Transfer Part B (1995) 353–369.

[15] D.C. Wilcox, Turbulence Modeling for CFD, DCW Industries, La Cañada, California, 1994.

[16] F.R. Menter, Eddy viscosity transport equations and their relation to the k–ε model, ASME J. Fluids Engrg. 119 (1997) 876–884.

[17] M. Nallasamy, Turbulence models and their applications to the prediction of internal flows: A review, Comput. Fluids (1987) 151–194.

[18] B.E. Launder, G.J. Reece, W. Rodi, Progress in the development of a Reynolds stress turbulence closure, J. Fluid Mech. 68 (1975) 537–566.

[19] V. Yakhot, S.A. Orszag, Renormalisation group analysis of turbulence, 1. Basic theory, J. Sci. Comput. 1 (1) (1986) 3–51.

[20] B.P. Leonard, A stable and accurate convective modeling procedure based on quadratic upstream interpolation, Comput. Methods Appl. Mech. Engrg. 19 (1979) 59–98.

[21] X.L. Luo, Operator-splitting computation of turbulent flow in an axisymetric 180° narrowing bend using several k–ε models and wall functions, Internat. J. Numer. Methods Fluids 22 (1996) 1189–1205.

[22] B.E. Launder, On the modeling of turbulent industrial flows, in: Hirsch, et al. (Eds.), Proceedings of Computational Methods in Applied Sciences, Elsevier, Amsterdam, 1992, pp. 91–102.

[23] D. Marchal, L'adhérence des jets d'air froid au plafond des locaux climatisés, Internat. J. Thermal Sci. (1999) 832–842.

[24] G.E. Myers, J.J. Schauer, R.H. Eustis, The plane turbulent wall jet, development and friction factor, Technical Report, Departments of Mechanical Engineering, Standford University, 1961.